

# Demonstration of focus-tunable diffractive Moiré-lenses

Stefan Bernet,\* Walter Harm, and Monika Ritsch-Marte

*Division for Biomedical Physics, Innsbruck Medical University,  
A-6020 Innsbruck, Austria*

*\*[stefan.bernet@i-med.ac.at](mailto:stefan.bernet@i-med.ac.at)*

**Abstract:** In an earlier publication [Appl. Opt. **47**, 3722 (2008)] we suggested an adaptive optical lens, which consists of two cascaded diffractive optical elements (DOEs). Due to the Moiré-effect the combined optical element acts as a Fresnel zone lens with a refractive power that can be continuously adjusted by a mutual rotation of the two stacked DOEs. Here we present an experimental realization of this concept. Four designs of these Moiré-DOEs (MDOEs) were fabricated in thin (0.7 mm) glass slides by lithography and subsequent etching. Each element was realized as a 16 phase level DOE designed for 633 nm illumination. Our experimental investigation shows that the Moiré-lenses have a broad adjustable refractive power range with a high efficiency, which allows one to use them for flexible beam steering and for imaging applications.

© 2013 Optical Society of America

**OCIS codes:** (050.1970) Diffractive optics; (120.3620) Lens system design; (090.1970) Diffractive optics.

---

## References and links

1. L. Guoqiang, "Adaptive lens," Progress in Opt. **55**, 199–283 (2010).
2. H. Ren, S. Xu, Y.-J. Lin and S.-T. Wu, "Adaptive-focus lenses," Opt. Photon. News 43–47 Oct. 2008.
3. G. Zhou, H. M. Leung, H. Yu, A. S. Kumar, and F. S. Chau, "Liquid tunable diffractive-refractive hybrid lens," Opt. Lett **34**, 2793–2795 (2009).
4. T. Nose, and S. Sato, "A liquid crystal microlens obtained with a non-uniform electric field," Liq. Cryst. **5**, 1425–1433 (1989).
5. S. Xu, Y.-J. Lin, and S.-T. Wu, "Dielectric liquid microlens with well-shaped electrode," Opt. Express **17**, 10499 (2009).
6. H. Ren, D. Fox, B. Wu, and S. T. Wu, "Liquid crystal lens with large focal length tunability and low operating voltage," Opt. Express **15**, 11328–11335 (2007).
7. P. Valley, D. L. Mathine, M. R. Dodge, J. Schwiegerling, G. Peyman, and N. Peyghambarian, "Tunable-focus flat liquid-crystal diffractive lens," Opt. Lett. **35**, 336–338 (2010).
8. P. J. Valle, V. F. Canales, and M. P. Cagigal, "Focal modulation using rotating phase filters," Opt. Express **18**, 7820–7826 (2010).
9. S. Bernet and M. Ritsch-Marte, "Adjustable refractive power from diffractive Moiré elements," Appl. Opt. **47**, 3722–3730 (2008).
10. S. Bará, Z. Jaroszewicz, A. Kolodziejczyk, and V. Moreno, "Determination of basic grids for subtractive Moiré patterns," Appl. Opt. **30**, 1258–1262 (1991).
11. Z. Jaroszewicz, A. Kolodziejczyk, A. Mira, R. Henao, and S. Bará, "Equilateral hyperbolic moiré zone plates with variable focus obtained by rotations," Opt. Express **13**, 918–925 (2005).
12. J.M. Burch and D.C. Williams, "Varifocal Moiré zone plates for straightness measurement," Appl. Opt. **16**, 2445–2450 (1977).
13. A. W. Lohmann, "A new class of varifocal lenses," Appl. Opt. **9**, 1669–1671 (1970).
14. A. Kolodziejczyk and Z. Jaroszewicz, "Diffractive elements of variable optical power and high diffraction efficiency," Appl. Opt. **32**, 4317–4322 (1993).

15. I. M. Barton, S. N. Dixit, L. J. Summers, C. A. Thompson, K. Avicola, and J. Wilhelmsen, "Diffractive Alvarez lens," *Opt. Lett.* **25**, 1–3 (2000).
16. S. Barbero, "The Alvarez and Lohmann refractive lenses revisited," *Opt. Express* **17**, 9376–9390 (2009).
17. S. Barbero and J. Rubinstein, "Adjustable-focus lenses based on the Alvarez principle," *J. Opt.* **13**, 125705 (2011).
18. T. Stone, N. George, "Hybrid diffractive-refractive lenses and achromats," *Appl. Opt.* **27**, 2960-2971 (1988).
19. R. Brunner, R. Steiner, H. J. Dobschal, D. Martin, M. Burkhardt, and M. Helgert, "New solution to realize complex optical systems by a combination of diffractive and refractive optical components," *Proc. SPIE* **5183**, 47-55 (2003).
20. G. I. Greisukh, E. G. Ezhov, A. V. Kalashnikov, and S. A. Stepanov, "Diffractive–refractive correction units for plastic compact zoom lenses," *Appl. Opt.* **51**, 4597–4604 (2012).
21. B. Kleemann, M. Seeßelberg, and J. Ruoff, "Design concepts for broadband high-efficiency DOEs," *JEOS - Rapid Pub.* **3**, 08015 (2008).
22. B. Kress and P. Meyrueis, *Digital Diffractive Optics* (Wiley, 2000).

## 1. Introduction

Lenses of adjustable refractive power, often called adaptive optical lenses, are highly desirable for many technical applications, for instance for imaging systems which mimic the function of the human eye or for adjustable illumination and beam steering [1, 2]. Therefore various systems have been developed, for example liquid-filled polymer vessels which change their shape, and accordingly their refractive power upon application of forces [1–3], or liquid crystal lenses which change their refractive index when a spatially controlled electric field [4–7] is applied.

In our approach we tailor the rotational Moiré effect, such that a combination of two DOEs forms a joint Moiré diffractive optical element (MDOE) with a variable refractive power of the resulting Fresnel lens, which can be adjusted by rotating one element with respect to the other around a central axis [8, 9], as indicated in Fig. 1. Similar approaches using absorptive

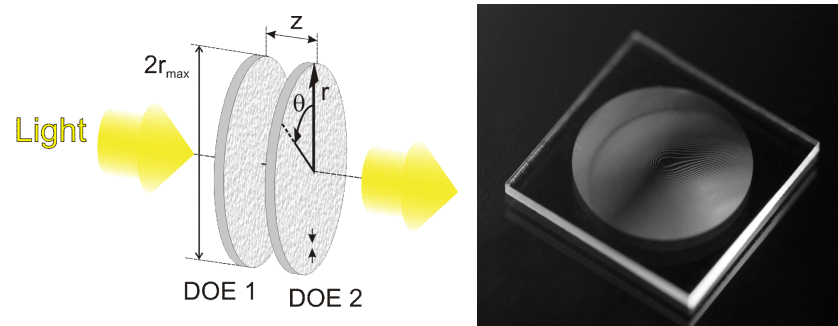


Fig. 1. Left: Operation principle of a MDOE: Two diffractive optical elements are combined into a "Moiré-lens" (not to scale). Rotating one of the elements with respect to the other by an angle  $\theta$  changes the optical power of the MDOE. Right: Photography of one of the produced DOEs, which - after combination with its counterpart - yields a Moiré-lens. The DOEs are realized as 16-level phase elements, etched into a glass plate (side length: 10 mm). The etched structure on the upper side is faintly visible by specular reflection of oblique illumination light.

Moiré-elements [10, 11], or Moiré-elements based on a lateral shift between the two combined DOEs [12–14], which are closely related to diffractive and refractive versions of the so-called Alvarez-lenses [15–17], have been described earlier. The MDOEs have the advantages of being thin elements (our assembled Moiré-lens has a thickness of 1.5 mm) while still having a high

adjustable refractive power range. This makes them usable in situations with strict space or weight limitations. Moreover, the focal length is precisely adjusted by the mutual rotation angle and remains fixed without applying an external throw force by using pressure or voltage. Thus the adjustment of the desired refractive power is precise and reproducible; once adjusted there is no subsequent "creeping" of the refractive power. The flatness of Moiré-lenses avoids lens-aberrations, and they even offer the possibility to design aspherical freeform lenses, which may be used to correct aberrations of standard lenses in a combined lens system.

On the other hand, there is the disadvantage that diffractive lenses are strongly dispersive, i.e. the refractive power depends linearly on the light wavelength. However, the dispersion is opposite to that of refractive (glass) optics, and therefore DOEs may be used for producing compound refractive/diffractive optical systems with reduced chromatic aberrations [3, 18–20]. Another disadvantage is that the diffraction efficiency of DOEs is limited. There are, however, methods to increase the efficiency even in a broadband wavelength range using compound DOEs [21]. With our prototype MDOEs we have achieved a maximal relative efficiency which is on the order of 85%.

## 2. Operation principle of Moiré-lenses

In our earlier publication [9] the principles for the design of Moiré-lenses were outlined. It was shown that any rotationally symmetric phase profile can be generated by placing two DOEs with conjugate phase profiles directly behind each other

$$\begin{aligned} T_1 &= \exp[iF(r)\varphi] \\ T_2 &= \exp[-iF(r)\varphi]. \end{aligned} \quad (1)$$

Here,  $r$  and  $\varphi$  are polar coordinates measured from the center of the optical element,  $F(r)$  is an arbitrary real function (e.g. a parabolic lens profile) which depends only on the radial coordinate  $r$  and is thus rotationally symmetric. Note that the two elements  $T_1$  and  $T_2$  are actually upside-down flipped versions of each other, since the coordinate transform for an upside-down flip means that  $r \mapsto r' = r$ , and  $\varphi \mapsto \varphi' = -\varphi$ . Therefore, for obtaining the pair of optical elements of Eq. (1), it is sufficient to produce two identical elements, flip one of them and put them together.

If  $T_2$  is rotated by an angle  $\theta$  around a central axis (i.e. around the point  $r = 0$ ), it transforms into

$$T_{2;\text{rot}} = \begin{cases} \exp[-iF(r)(\varphi - \theta)] & \text{for } \theta \leq \varphi < 2\pi \\ \exp[-iF(r)(\varphi - \theta + 2\pi)] & \text{for } 0 \leq \varphi < \theta. \end{cases} \quad (2)$$

The two cases have to be distinguished because of the  $2\pi$ -periodicity of rotations.

When placing the rotated second element on top of the first stationary DOE, the joint transmission function of the combination becomes  $T_{\text{joint}} = T_1 T_{2;\text{rot}}$ , which yields

$$T_{\text{joint}} = \begin{cases} \exp[iF(r)\theta] & \text{for } \theta \leq \varphi < 2\pi \\ \exp[iF(r)(\theta - 2\pi)] & \text{for } 0 \leq \varphi < \theta. \end{cases} \quad (3)$$

This means first, that the phase term in the exponent increases linearly with the rotation angle  $\theta$ , and second, that two different sectors (defined in Eq. (3)) are formed, consisting of transmission functions  $T_{j1} = \exp[iF(r)\theta]$  and  $T_{j2} = \exp[iF(r)(\theta - 2\pi)]$ , respectively, which in general have a different phase profile.

For generating a parabolic Fresnel zone lens we may use  $F(r) = F_{Fr}(r)$  with

$$F_{Fr}(r) = ar^2. \quad (4)$$

Here,  $r$  is the radial polar coordinate, and  $a$  is a selectable constant. According to Eq. (3), the joint transmission function of the two combined elements becomes

$$T_{\text{joint;Fr}} = \begin{cases} \exp[i\theta ar^2] & \text{for } \theta \leq \varphi < 2\pi \\ \exp[i(\theta - 2\pi)ar^2] & \text{for } 0 \leq \varphi < \theta. \end{cases} \quad (5)$$

Comparing this with the phase profile  $T_{\text{parab}}$  of a parabolic lens, namely with

$$T_{\text{parab}} = \exp\left[i\frac{\pi r^2}{\lambda f}\right], \quad (6)$$

where  $\lambda$  is the wavelength of the transmitted light, and  $f$  the focal length of the lens, one finds that Eq. (5) describes two parabolic lenses in the two sectors, with two different focal powers  $f^{-1}$  given by

$$\begin{aligned} f_1^{-1} &= \theta a \lambda / \pi & \text{for } \theta \leq \varphi < 2\pi & \text{ and} \\ f_2^{-1} &= (\theta - 2\pi) a \lambda / \pi & \text{for } 0 \leq \varphi < \theta. \end{aligned} \quad (7)$$

The difference between the refractive powers of the two lens sectors is constant and given by  $\Delta f^{-1} = f_2^{-1} - f_1^{-1} = -2a\lambda$ . Note that the resulting Moiré lenses in the two sectors are blazed Fresnel lenses, which can reach a diffraction efficiency close to unity.

For many applications it is desired that the entire area of the lens forms a uniform Fresnel zone lens without sectors. Due to the  $2\pi$  periodicity of the phase arguments in Eq. (3) this happens for any radial function  $F(r)$  which has a range of values consisting only of integer numbers, which is achieved with

$$F_{\text{iFr}}(r) = \text{round}\{ar^2\}. \quad (8)$$

Here,  $\text{round}\{\dots\}$  means rounding the arguments to the nearest integer number. According to Eq. (5) the resulting joint "integer" MDOE then has a uniform transmission function over its whole area

$$T_{\text{iFr}}(r) = \exp[i\theta \text{round}\{ar^2\}]. \quad (9)$$

Thus, the joint transmission function consists of a sequence of concentric annuli of constant phase, which become finer at the outer regions of the lens area. Between adjacent annuli there is always a fixed phase jump (i.e. a "digitalization step") of  $\theta$ . The refractive power in the first order of this joint lens corresponds to  $f_{+1}^{-1} = \theta a \lambda / \pi$ .

However, the digitalization of the phase term leads to a reduction of the diffraction efficiency in the desired first order, and to the appearance of non-zero diffraction intensity in the minus first diffraction order, which is superposed on the first lens. The appearance of the second superposed lens can be understood by noticing that the rounding operation of the phase term  $\theta \text{round}\{ar^2\}$  approximates the (first order) lens term  $\theta ar^2$  with a phase step size of  $\theta$ , and the (minus first order) lens term  $(\theta - 2\pi)ar^2$  with a different step size of  $2\pi - \theta$ . This is due to the  $2\pi$ -periodicity of the phase function, where a phase step of  $\theta$  (in positive direction) also corresponds to a phase step of  $2\pi - \theta$  in negative direction. Thus, the minus first order lens is an approximation to the phase term  $(\theta - 2\pi)ar^2$ , and has accordingly a refractive power of  $f_{-1}^{-1} = (\theta - 2\pi) a \lambda / \pi$ . Note that the same second lens term also appears in the non-integer variant of Moiré lenses described by Eq. (5).

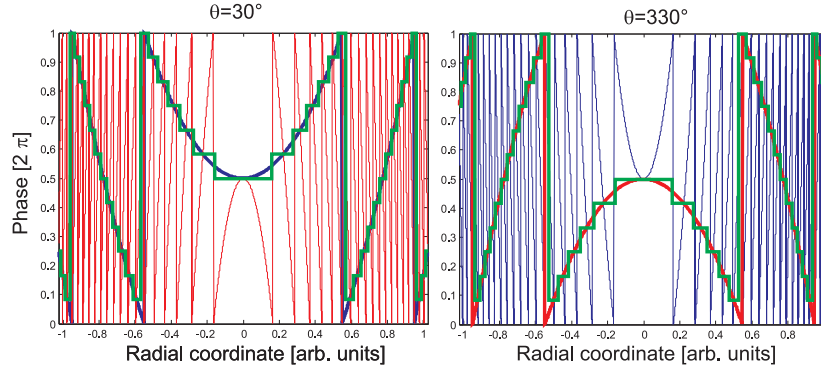


Fig. 2. Cross sections of the phase profiles of an integer Moiré lens (according to Eq. (9)) for two different relative rotation angles of  $30^\circ$  (left) and  $330^\circ$  (right). The green curve corresponds to the digitized phase profile according to Eq. (9), the blue curve to the first order lens with ideal blazed phase profile  $\theta ar^2$ , and the red curve to the minus first order lens with ideal blazed phase profile of  $(\theta - 2\pi)ar^2$ .

An illustration of this behavior is shown in Fig. 2. There the digitized phase profile  $\theta_{\text{round}}\{ar^2\}$  is plotted (green curves) for two different rotation angles  $\theta = 30^\circ$  (left) and  $330^\circ$  (right). In the case of  $\theta = 30^\circ$  (left), the ideal blazed phase profile  $\theta ar^2$  of the first order lens (blue) is approximated by the digitized curve (green) with a phase step size of  $\theta = 30^\circ = \pi/6$ , corresponding to a digital phase element consisting of 12 equidistant phase levels in each interval between 0 and  $2\pi$ . At the same time the approximation to the minus first order phase profile  $(\theta - 2\pi)ar^2$  (red curve) is poor, since the corresponding phase digitalization step  $2\pi - \theta \approx 1.83\pi$  creates a Fresnel zone lens consisting of (nominally) only  $2\pi/(2\pi - \theta) = 1.09$  phase levels.

The situation is inverted for rotation angles higher than  $180^\circ$ . As an example, the right hand side of Fig. 2 shows the corresponding phase profiles for a rotation angle of  $330^\circ$ . Now the minus first order lens profile (red) is better approximated. Note that for a rotation angle of  $\theta = 180^\circ$  the phase profile of the integer Moiré lens becomes binary, i.e. the phase step size is  $\pi$  for both of the superposed lenses, resulting in an equal superposition of two lenses with opposite sign of their refractive powers.

In order to calculate the expected diffraction efficiency  $\eta_1$  in the first diffraction order, the result for a standard  $N$ -level digital DOE is appropriate, given e.g. in Ref. [22] as

$$\eta_1 = \left( \text{sinc} \frac{\pi}{N} \right)^2. \quad (10)$$

In our case,  $N = 2\pi/\theta$  for the first order Moiré lens with phase profile  $\theta ar^2$ , and  $N = 2\pi/(2\pi - \theta)$  for the superposed lens  $(\theta - 2\pi)ar^2$ . Figure 3 shows the results of an analytical calculation (solid lines) according to Eq. (10), and of numerical calculations simulating our experimentally realized 16-phase level DOE structures. The numerical calculations were performed for a Moiré lens composed of two 16-level sub-DOEs with the phase transmission function of Eq. (8). As in the experiment, each DOE was defined by an array of  $4000 \times 4000$  square pixels. One of the arrays was numerically rotated with respect to the other by a certain angle  $\theta$ . Then the two transmission functions were multiplied, followed by numerical propagation (using a plane wave propagation operator) to its respective focal plane, where the intensity in the focus was determined.

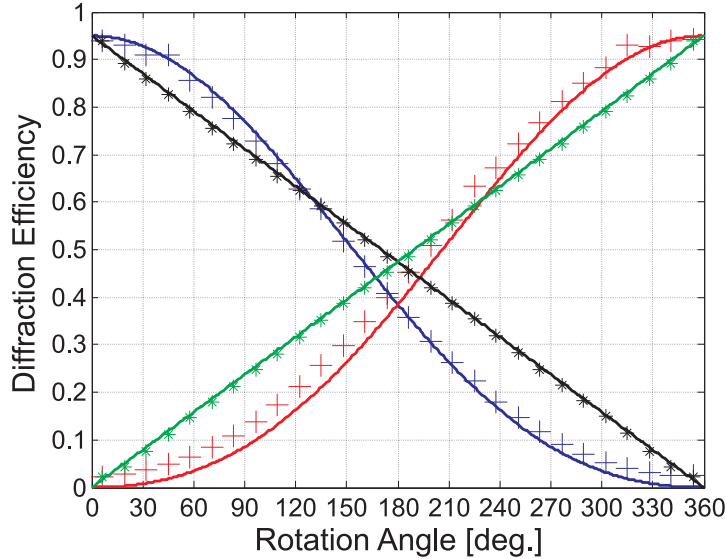


Fig. 3. Efficiencies of the two lens terms in the bifocal MDOE lenses as a function of the relative rotation angle  $\theta$ . Blue and red markers and curves correspond to numerical and analytical results for integer Moiré-lenses fabricated according to Eq. (8), respectively, whereas black and green marker and curves apply to a non-integer Moiré-lens according to Eq. (4).

It turned out that the numerically calculated efficiencies are 5% smaller than the analytical result according to Eq. (10) (in order to compare the shape of the corresponding curves, the analytic result was downscaled by this factor in Fig. 3). The reason for this is first, that the analytical result holds only for continuously blazed sub-DOEs, whereas the numerical calculation considers the 16 phase level digitalization, and second, that the rectangular structure of the basic grid produces artefacts when it is numerically rotated and then re-mapped into a new square array by interpolation. The numerical calculations show a maximal efficiency of about 94% for the first order integer Moiré lens (blue curve) at zero rotation angle, which decreases to 78 % at a rotation angle of  $90^\circ$ . In the same rotational range the efficiency of the minus first order integer MDOE lens increases from 0 to 9% (red curve). For many applications the moderate efficiency loss of less than 20% in the rotational range between  $-90^\circ$  and  $+90^\circ$  may be acceptable, and thus we define this as the "efficient" tuning range. For a non-integer MDOE with sector formation, the relative efficiencies of the two lens terms appearing in the two separated sectors depend only on the areas covered by the respective sectors, such that the efficiencies are a linear function of the rotation angle (black and green curves).

The maximum diffraction efficiency is always obtained at a rotation angle of  $0^\circ$ , which corresponds (according to Eq. (7)) to zero refractive power. In many applications, however, it is desired to have the maximum efficiency at a certain "offset" refractive power. This can be realized by superposing an offset Fresnel zone lens on any (or both) of the two DOE elements. In order to keep the combined DOEs still symmetric with respect to an upside-down flip, we choose the two transmission functions according to

$$\begin{aligned} T_{iFr1}(r) &= \exp[i\varphi \text{round}\{ar^2\} + ibr^2] \quad \text{and} \\ T_{iFr2}(r) &= \exp[-i\varphi \text{round}\{ar^2\} + ibr^2]. \end{aligned} \quad (11)$$

Note that the usable range of the constants  $a$  and  $b$  in Eq. (11) is limited in order to avoid undersampling, as outlined in [9]. Combining these two transmission functions, one obtains an integer Moiré lens which has basically the same features as described before (Eq. (9)), but with an offset refractive power  $f_{\text{offset}}^{-1}$  of

$$f_{\text{offset}}^{-1} = 2b\lambda/\pi. \quad (12)$$

The efficiency of this Moiré lens as a function of the relative rotation angle corresponds to that plotted in Fig. 3, i.e. the maximal efficiency is again obtained at zero rotation angle, where an offset refractive power of  $f_{\text{offset}}^{-1}$  is present.

### 3. Experimental results

The "sub-DOEs" from which the MDOEs are assembled were fabricated as contracted work by a specialized company. In order to calculate the phase masks, the phase terms in all of the above listed transmission functions were taken "modulo  $2\pi$ " (i.e. "blazed"), and then digitized to obtain 16 phase levels. The phase masks were calculated as square pixel arrays consisting of  $4000 \times 4000$  (designs 1-3), or  $6000 \times 6000$  (design 4) pixels. The size of each pixel in designs 1-3 was chosen to be  $2\mu\text{m} \times 2\mu\text{m}$ , and  $1\mu\text{m} \times 1\mu\text{m}$  in design 4. A photograph of one of the phase plates (element 2) is shown in Fig. 1. We produced four different types of Moiré lenses. All of them were produced in fused silica plates (thickness: 0.7 mm) by lithography (using a 4-step binary mask exposure process of a single waver containing 200 individual DOEs), and subsequent etching as 16 phase level blazed DOEs, i.e. with 16 equidistant phase jumps in an interval between 0 and  $2\pi$ , optimized for an illumination wavelength of 633 nm. According to atomic force microscopy measurements performed by the company, the variations of the etch depths of the four layers around their targeted depths are:  $692\text{ nm} \pm 1.3\%$ ,  $346\text{ nm} \pm 1.2\%$ ,  $173\text{ nm} \pm 1.4\%$ , and  $86.5\text{ nm} \pm 4.5\%$ , respectively, and the overlay error of the 4-mask alignment process is smaller than 70 nm between subsequent layers.

The detailed properties of the four different DOEs are listed in Fig. 4. The table provides information about the resolution (array size), the size of the individual square pixels, the diameter of the circular elements, and the production "recipe", i.e. the corresponding equation which describes the phase profile, and the constants used in these equations. The nominal tuning range of the refractive power is quoted for a full rotation between 0 and  $360^\circ$ . However, as mentioned earlier, the "efficient" tuning range between  $-90^\circ$  and  $+90^\circ$  (with only a moderate efficiency reduction of less than 20%) reduces the efficient accommodation range to 25% of the listed values, e.g. for element 4 it ranges from -26 to +26 diopters (dpt).

A sketch of elements 1-3 (not to scale, resolution decreased) is shown in the right column of Fig. 4. There, gray levels correspond to phase levels in an interval between 0 and  $2\pi$ . Since element 4 is basically the same as element 2 (with increased resolution), the image in the fourth row shows as an example the *combined* Moiré-lens at a relative rotation angle of  $45^\circ$ , which yields the blazed phase profile of a uniform Fresnel lens.

A photograph of one of the assembled non-integer Moiré lenses (element 1) in a homebuilt rotational sample holder is shown in Fig. 5. The lens was placed about 4 cm above a text fragment acting as a sample, which was illuminated by a halogen lamp with an additional red filter (bandwidth on the order of 30 nm). The sector marked red indicates the mutual rotation angle of about  $75^\circ$  between the two stacked DOEs. As expected for the non-integer Moiré lens (element 1), two different lens sections are created inside and outside of the marked sector, with corresponding refractive powers of approximately -32 dpt, and +8 dpt, respectively (see Eq. (7)). This results in a demagnification of the sample text seen through the marked sector and a (slight) magnification outside. Within each of the two different sectors, the experimentally measured relative diffraction efficiency is on the order of 85%.

No.	Array size (N x N)	Pixel size (μm)	Diameter (cm)	Constants (m <sup>-2</sup> )	f <sup>-1</sup> -range (m <sup>-1</sup> )	Features
1	4000 x 4000	2.0	0.80	a=3.12 x 10 <sup>7</sup>	-40 ... +40	Non-integer Moiré lens (with sector formation, Eq.4)
2	4000 x 4000	2.0	0.80	a=3.12 x 10 <sup>7</sup>	-40 ... +40	Integer Moiré lens (Eq. 8)
3	4000 x 4000	2.0	0.80	a=3.12 x 10 <sup>7</sup> b=2.45 x 10 <sup>7</sup>	-30 ... +50	Integer Moiré lens with offset 10 dpt (Eq. 11)
4	6000 x 6000	1.0	0.60	a=8.33x 10 <sup>7</sup>	-104... +104	Integer Moiré lens (Eq. 8)

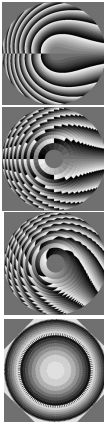


Fig. 4. Properties of the four produced MDOEs. All of them are etched in fused silica as 16 phase level DOEs. The right column shows a magnified sketch of the central region of the phase masks (not to scale, gray values correspond to phase levels). Element 4 is practically the same as element 2 (with smaller pixel size), therefore - for additional information - the sketch at the right shows as an example the resulting stacked Moiré lens at a mutual rotation angle of 45°.

The other three lens types are constructed according to Eq. (8) as "integer" Moiré lenses, which avoid the sector generation of element 1. All of these produce uniform bifocal Moiré lenses (as can be seen in the fourth row of table 4), where the efficiencies and the focal length of the two superposed lens terms depend on the rotation angle, as shown in Fig. 3.

The refractive powers and the diffraction efficiencies of all Moiré elements were experimentally determined as a function of the rotation angle. For illumination, an expanded, collimated HeNe-laser beam (633 nm) was used. For positive refractive powers, a focal spot could be observed behind the MDOE lenses, where an iris (diameter 1.0 mm) was placed which just transmitted the light in the focus. Behind the iris, the transmitted light power was measured with a powermeter. The procedure of finding the focal spot and centering it with the iris had to be repeated for different rotation angles of the Moiré lenses. The distance between lens and focal spot was measured in order to obtain the focal length as a function of the rotation angle, and plotted in Fig. 6. The measured light power behind the iris was normalized by the power measured directly behind the Moiré lens, which yields the relative diffraction efficiency as a function of the corresponding refractive power, i.e. the amount of light focused by the MDOE lens compared to the total transmitted light.

Figure 6 shows the measured refractive powers of all Moiré lenses as a function of the rotation angle. As expected, the MDOEs 1 (red), 2 (blue) and 3 (green) show the same change of the refractive power per angular rotation, namely 0.11 dpt/degree, such that a rotation in the "efficient" range between -90° and +90° corresponds to an accommodation range of 20 dpt. The data for element 3 (green) is shifted with respect to the data for elements 1-2, as expected, since it has an offset refractive power of 10 dpt. The data for element 4 (black) shows another slope of the refractive power change, namely 0.28 dpt/degree, due to the different choice of the constant  $a$  in Eq. (8).

The plot at the right side of Fig. 6 shows the relative diffraction efficiencies of the Moiré lenses measured as a function of the corresponding refractive powers. The data have been fitted

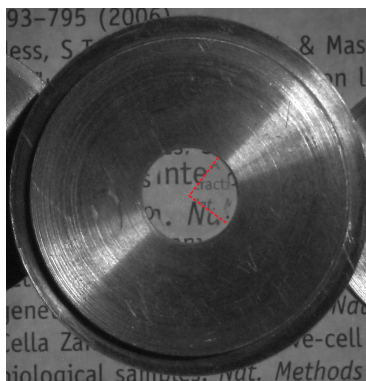


Fig. 5. Photograph of a non-integer Moiré lens according to design 1, mounted in a home made rotation stage and placed about 4 cm above a page of sample text. The mutual rotation of the two assembled DOEs of about  $75^\circ$  corresponds to the opening angle of the red marked sector. As expected for the non-integer Moiré element 1, two Fresnel lenses with different refractive powers are created inside and outside of the marked sector resulting in a demagnification and magnification of the sample text observed through the respective lens areas. A further rotation of one DOE with respect to the other would increase the size of the marked sector, and simultaneously change the refractive powers within and without the sector according to Eq. (7).

with the expected models, i.e. a linear behaviour for element 1, and a "sinc<sup>2</sup>"-behavior according to Eq. (10) for the elements 2-4. In our experimentally accessible refractive power range, the shape of the curves roughly agrees with the expectations, but with a significantly lower peak efficiency. Note that element 3 (green) reaches its peak efficiency at a refractive power of 10 dpt, as expected due to the offset lens term. For element 4 (black) the decrease in efficiency with increasing refractive power is lower than that for the other elements, due to the fact that element 4 is designed to cover an increased accommodation range at the cost of a higher pixel resolution. Element 1 (red) shows the expected linear behavior only for the refractive power range higher than 5 dpt, which may be due to alignment tolerances of our prototype MDOE mount. According to our numerical simulations the maximal efficiencies of all elements should reach about 94%, whereas the experimentally measured peak efficiencies are 86%, 72%, 69%, and 81% for the MDOEs 1, 2, 3, and 4, respectively. One reason for the decreased experimental efficiency may be due to production tolerances in the etched phase plates. In our case, possible phase errors are more problematic than for standard diffractive lenses, since their effect adds up in the stacked elements.

However, a more important source for the efficiency reduction may be a misalignment in axial direction. Ideally, the two DOEs within a Moiré lens should be placed directly on top of each other, with no axial distance. However, in our prototype rotation mounts the axial distance can be only controlled with a quite large tolerance on the order of  $50 \mu\text{m}$ . Numerical simulations show that the efficiency decrease in the case of an axial misalignment is more severe for the integer Moiré elements 2-4, than for the non-integer element 1, due to the fact that the rounding operation of the integer elements produces more (non- $2\pi$ -) phase jumps, where light is significantly scattered if the distance to the second DOE exceeds the Talbot length ( $L_{\text{Talbot}} = 2p^2/\lambda$ , where  $p$  is the pixel size of the MDOE) [9]. This would agree with the experimental observation that the efficiency of the non-integer Moiré lens 1 comes closer to its theoretically expected value.

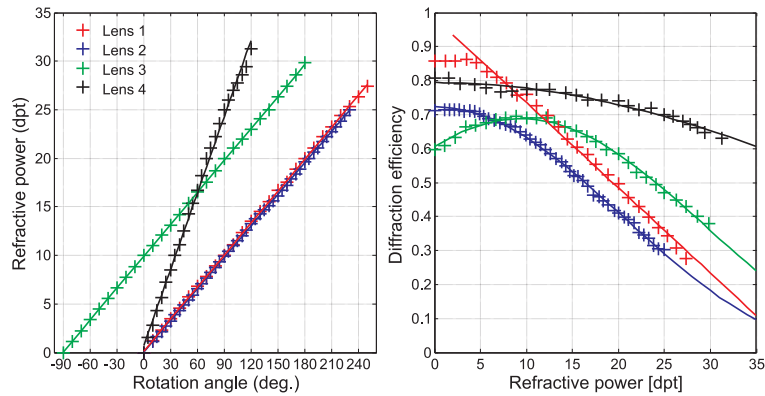


Fig. 6. Left: Experimentally measured dependence of the refractive powers of the 4 different Moiré lenses as a function of the rotation angle. The continuous lines are a linear fit to the data. Right: Relative diffraction efficiencies of the Moiré lenses as a function of their measured refractive powers. The black, blue and green continuous curves for the integer Moiré elements are fits to the data according to Eq.(10).

For investigating the effects of *lateral* misalignment of the Moiré elements, a mechanical holder was assembled which allowed both, a rotation of one DOE element with respect to the other, and a lateral shift between the two elements with 0.5 micron precision. Centering of one DOE plate with respect to the other was performed under visual inspection through a microscope, using the fact that the central pixel of each DOE could be identified. Using this mount, the relative diffraction efficiency of a Moiré lens could be measured as a function of the lateral displacement (“decentering”) between the two DOEs. We imaged the point spread function (PSF) of the lens using a camera with a linear intensity response (PCO 4000s, 14 bit depth resolution) in the rear focal plane of the Moiré lenses, which were once again illuminated with an expanded, collimated HeNe laser beam. The results are shown in Fig. 7.

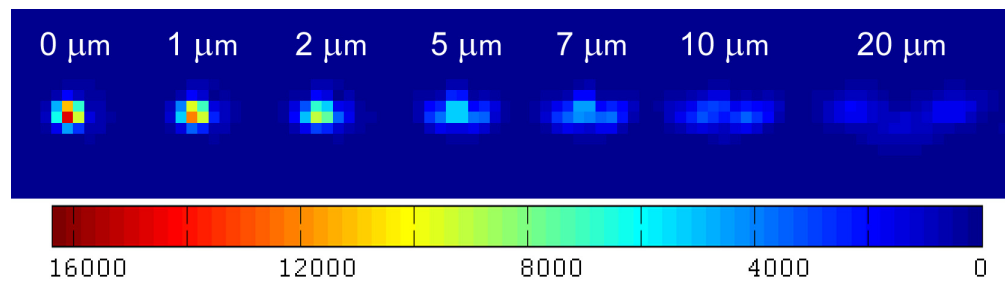


Fig. 7. Point spread functions of Moiré lens 2 as a function of the lateral misalignment of the two stacked DOEs. The focal length of the lens was adjusted to 20 cm, and the intensity in the focal spot was imaged with a camera (ccd pixel counts are coded according to the colorbar below). One square camera pixel had a size of  $9\mu\text{m} \times 9\mu\text{m}$ . The data shows that for perfect alignment (left image) a diffraction limited PSF is produced, with a width on the order of  $10\mu\text{m}$ . For increasing misalignment (lateral misalignment between centers of the two DOEs indicated in the images) the PSF starts to split into two separated spots.

The left image shows the result for the optimally centered Moiré lens (element 2). The camera pixels which are visible in the image have an edge length of  $9\ \mu\text{m}$ . The measured PSF has a width on the order of  $10\ \mu\text{m}$ . Since the MDOE lens has a radius of  $4\ \text{mm}$ , the corresponding numerical aperture (NA) at the focal distance of  $20\ \text{cm}$  is  $0.02$ , which results, according to  $w = \lambda/\pi\text{NA}$ , in a focused beam waist  $w$  of an incident Gaussian beam of  $10\ \mu\text{m}$ . Thus, for optimal alignment the Moiré lens produces a diffraction limited PSF. For increasing misalignment the PSF shows a continuous broadening in the direction of the decentering (horizontal). A considerable degradation of the PSF is observed at a misalignment of  $7\ \mu\text{m}$  (fifth image from the left). There the PSF becomes an ellipsoid which expands about  $60\ \mu\text{m}$  along the horizontal direction. For even larger misalignment (e.g.  $20\ \mu\text{m}$  for the right image in Fig. 7), the PSF starts to split into two spots (in this case separated by about  $90\ \mu\text{m}$ ). For further misalignments (not shown), the separation between these two spots increases linearly. A lateral displacement into the opposite direction results in a symmetric change of the PSF. The results shows that the effect of misalignment is "benign", i.e. the quality of the PSF reduces just gradually with increasing decentering.



Fig. 8. Test images recorded with Moiré lenses used as camera objectives. (a): Monochrome image (illumination at  $633\ \text{nm}$  with a HeNe laser) of a USAF resolution target placed at a distance of  $11.0\ \text{cm}$  in front of Moiré element 4 (diameter:  $6\ \text{mm}$ ). Distance between lens and camera chip was  $19.2\ \text{cm}$ , and the focal length of the Moiré lens was adjusted to  $7.0\ \text{cm}$ . The line pairs in group 5, element 5 are still resolved, corresponding to a resolution of  $50$  line pairs per  $\text{mm}$ . (b) White light image of two toy cars placed at a distance of  $22\ \text{cm}$ , and  $54\ \text{cm}$  in front of Moiré element 2 ( $8\ \text{mm}$  diameter), respectively. The distance between lens and camera chip was  $20\ \text{cm}$ . In (b) the focal length of the Moiré lens was adjusted to  $10.5\ \text{cm}$ , thus focusing on the nearer car. In (c) the focal length was changed to  $14.5\ \text{cm}$ , focusing on the other toy car.

Figure 8 shows images recorded with two different Moiré elements acting as objective lenses in front of an "open" CMOS camera (Canon EOS 1000D with removed objective, chip size  $22.3 \times 14.9\ \text{mm}^2$ ). In (a) the resolution achievable with Moiré element 4 (diameter:  $6\ \text{mm}$ , efficient tuning range:  $-26\dots+26\ \text{dpt}$ ) was tested by imaging a USAF resolution target with laser light at  $633\ \text{nm}$ , which was first transmitted through a rotating diffuser disc in order to suppress speckle. The distances between the sample, the lens, and the CMOS chip were chosen to be  $11.0\ \text{cm}$  and  $19.2\ \text{cm}$ , respectively, and the focal length of the Moiré lens was adjusted to  $7.0\ \text{cm}$ . An USAF element (element 5 in group 5) with a resolution of  $50$  line pairs per millimeter is just resolved, corresponding to an experimentally achieved resolution of about  $20\ \mu\text{m}$ . This is comparable to the expected diffraction limited resolution of  $23\ \mu\text{m}$ , which results from the geometry of the setup (imaging  $\text{NA}=0.027$ ,  $\lambda=633\ \text{nm}$ ). Note that - although the used Moiré lens is actually a bifocal lens - there is almost no contrast reduction due to the superposed other lens term. This is due to the fact that the two superposed lenses have very different refractive

powers, i.e. if one of them focuses an image, the other produces only a weak background which is diffusely distributed over an area larger than the (typical) image plane.

In (b) and (c) the Moiré lens 2 (diameter: 8 mm, efficient tuning range: -10 ... +10 dpt) is used for white light imaging. In this case, two toy cars were used as sample objects, placed at distances of 22 cm and 54 cm from the lens, respectively. The distance between lens and camera chip was adjusted to 20 cm. In (b) the focal length of the Moiré lens was adjusted to 10.5 cm, resulting in a sharp image of the nearest toy car. In (c) the focal length of the Moiré lens was changed to 14.5 cm, producing a sharp image of the second toy car, while the first one becomes blurred. The images show that dispersion due to diffraction at the Fresnel lenses reduces the image quality, but to a degree which may still be acceptable for various applications. Chromatic effects can also be compensated, when necessary, by attaching the diffractive Moiré lens to plano-convex or -concave refractive lenses (e.g. used to create the offset refractive power). Our experiments demonstrate the feasibility of Moiré lenses to act as imaging objectives with a fixed distance between lens and camera chip, which can refocus by just adapting the focal length, similar to imaging in the human eye.

#### 4. Conclusion

We have experimentally investigated the properties of a prototype set of 4 different Moiré lens elements, all fabricated as pairs of 16 phase level DOEs. Our experiments clearly demonstrate that it is possible to use this approach to create varifocal diffractive lenses. The imaging quality of the assembled Moiré elements was good, characterized by a diffraction limited point spread function. Chromatic effects decrease the image quality, but could be reduced by reverting to combinations with a refractive element of opposite dispersion. The experimental data for refractive power and diffraction efficiencies as a function of the mutual rotation angle match the predictions of numerical simulations for 16 level DOEs generally very well. The experimentally measured efficiencies of all 4 lens types, however, were somewhat lower than the numerically expected efficiencies for ideal elements, which is probably due to fabrication tolerances of the elements, and due to axial positioning tolerances of the DOE pairs, which still promises a potential for further efficiency gain. We have also shown that the contrast reduction stemming from the bifocal nature of the MDOE lenses is rather low, because light diffracted by the undesired lens terms is strongly defocused and thus "diluted" in the image plane. An alternative which avoids a bifocal lens is to use the non-integer Moiré lens design of element 1, and to shield the undesired sector by a corresponding absorptive mask.

The key advantage of a Moiré lens for imaging is that focusing requires no shift of the lens, as necessary in conventional objectives. The working principle of such an imaging system is thus similar to that of the eye. Since the distance between camera sensor and Moiré lens remains constant, the image magnification is inversely proportional to the distance of an object to the lens - this behaviour is different from that of a standard camera, and may be advantageous in quantitative applications, like production control. If, however, also an axial shift of the Moiré lens is possible, a single-lens zoom objective becomes feasible. Furthermore, a combination of two or more MDOEs allows for the construction of new types of optical systems, like zoom objectives, microscopes or telescopes with variable magnification, which do not require any axial shift of their components.

#### Acknowledgments

This work was supported by the "PRIZE 2010" program of the Austrian Federal Ministry of Economy, Family, and Youth (BMWFJ), Project No. Z100379. We also appreciate the valuable support in project management by Mag. Peter Buchberger from *transidee gmbH* (Transfer Center University of Innsbruck).